Bitumen fractionation: contribution of the individual fractions to the mechanical behavior of road binders

Emmanuel Chailleux, Clémence Queffelec, Ilef Borghol, Fabienne Farcas, Sandrine Marceau, Bruno Bujoli

Bitumen fractionation: contribution of the individual fractions to the mechanical behavior of road binders

Emmanuel Chailleux,[a]* Clémence Queffélec,[b]* Ilef Borghol,[a,b] Fabienne Farcas,[c] Sandrine Marceau,[c] and Bruno Bujoli[b]

[a] *MIT, Univ Gustave Eiffel, Ifsttar, Route de Bouaye CS4, 44344 Bouguenais, France*

[b] *Université de Nantes, CNRS, CEISAM UMR 6230, F-44000 Nantes, France*

[c] *CPDM, Univ Gustave Eiffel, IFSTTAR, F-77454 Marne-la-Vallée, France*

∗ Corresponding authors: emmanuel.chailleux@ifsttar.fr, clemence.queffelec@univ-nantes.fr

Abstract

Anticipation of alternative road binder to replace petroleum derived bitumen requires a deep understanding of the relations between the chemical composition of bitumen and the physical properties, especially rheological properties. The exact molecular structure of the vast number of different molecules constituting bitumen is too complicated to unravel, thus in this paper we propose to fractionate bitumen into four fractions and study their different physico-chemical properties. The melting temperature and the glass transiion of each fractions was determined by DSC while their molecular weight distribution was determined by HS-SEC. Finally, their rheological properties were investigated by DSR. This study highlighted the importance of all bitumen phases: the less polar liquid phase driving the viscous behavior up to -50 °C, the more polar solid phase responsible of the thermal stability and the stiffness, and finally the

intermediate viscous oily phases allowing the molecular weight distribution continuity and by consequence allowing to have, on a large temperature range, a viscous liquid behavior at high temperature or low frequency, and an elastic stiff behavior at low temperature. Crystallizable fractions and asphaltene aggregates seemed to act as key molecular structures in the continuous phase.

Keywords: Bitumen, fractionation, rheological behavior, GPC, asphaltenes, maltenes, DSC

1. Introduction

Bitumen is a by-product resulting from the vacuum distillation of petroleum crude oil. This organic material which is used for many building applications (road paving, waterproofing, roofing, corrosion protection…), is a material that consists of a high number of organic compounds structured in a very complex form. Its elemental composition depends on its geographical source, but mainly includes carbon (80- 88 wt.%) and hydrogen atoms (8- 12 wt.%) with a hydrogen-to-carbon molar ratio (H/C) of 1.5, in addition to a small amount of heterocyclic species and functional groups containing sulphur, nitrogen and oxygen atoms [1,2].

It is almost impossible to obtain an extensive chemical characterization of a bitumen and its composition is still debated. Bitumen are mainly composed of asphaltenes and maltenes. Asphaltenes are defined, according to the Standard NF T60-115 [3], as the fraction which is insoluble in *n*-alkanes and appear as solid black particles built of polar aromatic ring systems and heteroatom polar functional groups [2,4]. Different descriptions were proposed for asphaltenes. Yen [5-7] proposed a structural model based on layered building units composed of polycondensed aromatic rings substituted by aliphatic chains and naphthenic polycyclic rings. These building units can then be found under their monomeric form or self-assembled as

particles made of clusters of 3 to 5 layers, micelles comprising 2 or 3 particles, and finally larger aggregates composed of an ensemble of particles and micelles. Yen's model was then revised by Mullins [8] who reported three aggregation states for asphaltenes molecular structures in solution (Figure 1): (i) monomers, in agreement with the Yen's representation, (ii) nanoaggregates having an aggregation number of 6 and (iii) clusters consisting of 8 nanoaggregates formed for asphaltenes concentration in the range of a few grams per liter.

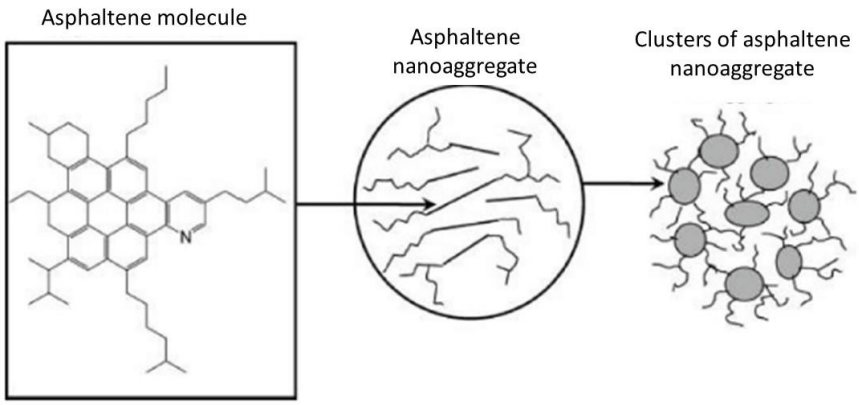

Figure 1. Three aggregation states of molecular structures of asphaltenes in solution according to Mullins [8]

Asphaltenes aggregation is driven by different intermolecular interactions, including π-π stacking between aromatic sheets and hydrogen bonding between functional groups [9]. Thanks to recent developments in characterization techniques, the average molecular weight of asphaltenes was estimated to be 750 Da, with most of the population between 500 and 1000 Da [10,11]. For what regards the arrangement of these species in bitumen [12], Nellensteyn [13,14] proposed in 1923 that asphaltenes form a colloidal suspension within the maltene phase, in which asphaltene micelles are surrounded by resins that act as peptizing agents and create a solvation layer that prevents aggregation. In 1940, Pfeiffer and co-workers [15] suggested two types of bitumen configuration to rationalize its viscoelastic properties: (i) a sol configuration

and (ii) a gel configuration (**Erreur ! Source du renvoi introuvable.**2). The former case is characterized by the presence of enough resin and aromatic molecules to completely solvate and peptize the asphaltenes molecules, so that micelles exhibit a high mobility and bitumen a Newtonian behavior. The latter case is characterized by an insufficient amount of resin and aromatic molecules resulting in fully interconnected asphaltenes micelles and a non-Newtonian bitumen behavior.

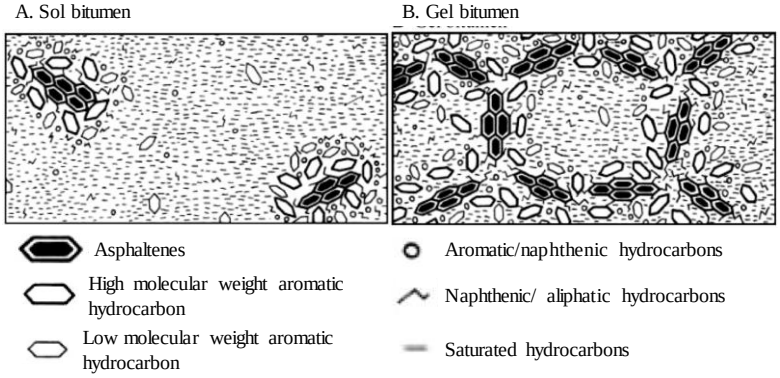

Figure 2. The bitumen colloidal model: Sol (A) and gel (B) configurations (adapted from [2])

Most bitumen show an intermediate behavior between these two types of configuration [12] called the sol-gel bitumen structure. In 1994, in a SHRP report[16] was proposed the Dispersed Polar Fluid (DPF) model that was then confirmed by Redelius [17]. Instead of considering bitumen as a colloidal dispersion, this model is based on the idea that the bitumen stability arises from the continuum of polarities and sizes of its constituting molecules. In this approach, the viscosity at high service temperatures results from London Dispersive interactions, which can be estimated from the molecular weight, and the amount of large polycyclic aromatic systems. At lower temperatures, other factors start to influence the behaviour, such as polar interactions, or wax which starts to crystallize.[18] In fact, at low temperatures, the bitumen viscoelastic response is the result of the strength of polar interactions between molecules. At

high temperatures, the bitumen Newtonian behavior is explained by the increase of polar interactions and the thermal energy.

The most common method to investigate the composition of bitumen is to fractionate it into different components and study each of those components separately. In this context, Corbett first proposed in 1969 [19] to use *n*-heptane to separate asphaltenes which are insoluble in that solvent. Then, liquid chromatography was performed on the soluble part (maltenes) to separate three fractions of different polarity: saturates (elution with *n*-heptane), aromatics (elution with toluene) and resins (elution with a 50/50 mixture of toluene and methanol). This method has established as one of the reference method for the bitumen fractionation (ASTM D-4124) [20] (SARA fractions for Saturates, Aromatics, Resins and Asphaltenes). It has to be noted that more recently, similar methodology using different solvents has been developed to separate maltenes in six fractions.[21]

Interestingly, sustainable routes towards bitumen substitutes have been investigated, either for its full replacement or for the production of additives capable to improve the performances of road binders [21-24]. As the composition of these substitutes markedly differs from that of traditional bitumen, it is of high interest for the development of alternative materials to understand the relation between the respective physicochemical data of bitumen main components and the rheological properties of the binder.

In this context, a 35/50 grade standard road binder was fractionated into four components which were characterized in terms of molecular weight distribution, phase changes and viscoelastic properties to assess the individual contribution of each of these components to the overall rheological behavior of the bitumen.

2. Materials and methods

2.1. Materials

A 35/50 penetration grade conventional bitumen from direct distillation was used in this study. Conventional properties are given in Table 1.

Table 1. Bitumen conventional properties.

Penetration@ 25° (1/10 mm) (EN 1426)	Softening point (°C) (EN 1427)	SARA fractions (%) (NF T 60-115)
38	53.6	S = 7.8 ± 0.7 A = 50.3 ± 2.8 R = 24.2 ± 1.8 C7-Asp = 17.7 ± 1.7

S : Saturated; A: Aromatics; R : Resins; Asp: Asphaltenes

SARA fractions from Table 1 were obtained by first c7-asphaltene precipitation in n-heptane. Then, maltenes were separated as followed: saturates were eluted in a solution of n-heptane; moreover, a solution of toluene/n-heptane (80/20 by volume) was introduced to elute the aromatics. Resins were determined by an elution in dichloromethane/methanol (95/5 by volume).

2.2. Bitumen fractionation procedure

2.2.1. General chemistry

The chromatography steps included in the bitumen fractionation process were performed using silica 60 M from Macherey-Nagel and neutral aluminium oxide from Carlo Erba. HPLC grade

solvents (i.e. pentane, dichloromethane, methanol and cyclohexane) were obtained from Aldrich, Acros or Alfa Aesar, and used without further purification for the fractionation procedure.

2.2.2. Fractionation steps

The asphaltene and maltene fractions were first separated by mixing bitumen (17 g) and n-pentane (550 mL). The mixture was stirred and refluxed for 1 h, and the n-pentane insoluble fraction (C5-asphaltenes, named in the following C5-A) was filtered on a PVDF membrane (pore size diameter: 0.22 µm), and dried in an oven at 80 °C for 16 h, leading to a black powder (5.5 g). After evaporation of the solvent under reduced pressure, the n-pentane soluble fraction corresponding to maltenes was separated into three other fractions by successive chromatography. In a first step, 450 g of neutral alumina were used to elute a first fraction (F1F2) using 1800 mL of dichloromethane. Then, the more polar fraction (F3), was eluted with 410 mL of a 60/40 v/v dichloromethane/methanol mixture and evaporated to yield a thick black oil (1.5 g). In a second step, the F1F2 less polar product was chromatographed on 180 g of silica to obtain a low polarity fraction (F1) using 3 L of cyclohexane leading to a yellow-orange oil after evaporation (6.1 g). A second fraction of intermediate polarity (F2) was then eluted using 1100 mL of a 60/40 v/v dichloromethane/cyclohexane mixture. After evaporation of the solvents, F2 was isolated as a dark brown oil (3.8 g). **Erreur ! Source du renvoi introuvable.** in the supporting information summarizes the fractionation procedure performed in this study.

2.4. Characterization methods and techniques

2.4.1. Fourier transform infrared spectroscopy (FT-IR).

The ATR-FTIR spectra were obtained in the 600- 4000 cm^{-1} range with a Bruker Vector 22 FTIR spectrometer and the OPUS software was used to process the data.

2.4.2. High-speed size exclusion chromatography (HS-SEC).

In this study size exclusion chromatography was used in high-speed conditions to quantify isolated molecules but also molecular associations. Indeed, SEC is conventionally used to separate and quantify molecules in a mixture depending on their size [25,26]. However, in order to highlight asphaltene associations, Brûlé et al. [27] analyzed bitumen in the particular conditions of HS-SEC (high flow and high concentration). This use of the SEC provides the closest possible chromatographic picture of the assumed colloidal structure of bitumens.

Analyses were performed using a Waters 510 solvent delivery system and a Waters 486 UV detector at a wavelength of 340 nm and separations were performed with a 500 Å Waters µ-styragel divinylbenzene chromatographic column (30 cm, 7.8 mm) with a particle size of 10 µm. 10 µL of the bitumen fractions diluted in tetrahydrofuran (THF, HPLC grade provided by SDS) at a concentration of 15 g/L were injected. THF (THF, HPLC grade provided by SDS) was used as an eluent at a flow rate of 3 mL/min.

The calibration curve was obtained from polystyrene standard samples with Mw values of 500 800, 52 000, 22 000, 9 200, 5 050, 2 950 and 1 700, supplied by Polymer Laboratories. Cyclopentane (Mw :70) was used for the determination of the total permeation volume. The exclusion volume (V_0) and the total permeation volume (V_{tot}) of the column were 5.7 mL and 10.6 mL, respectively. Molecular weights above 43 000 were excluded from the stationary phase pores, and molecular weights below 90 were eluted at total permeation volume. The polystyrene standard are probably not the ideal standard because their structure are different from molecules in bitumen. However, this calibration method is the most commonly used. The measured molecular weights are not exact but allow comparison of the weight distributions of the bitumen and its fractionation products.

2.4.3. Differential scanning calorimetry (DSC).

All measurements were carried out on a DSC Q100 TA instrument. 10 mg of each sample were encapsulated in sealed pans that were then heated to 180 °C at a 10 °C min^{-1} rate once the temperature was stabilized at 25 °C. Then, the sample was cooled down to 40 °C at a 10 °C min^{-1} rate, down to -40 °C at a 1 °C min^{-1} rate, and finally down to -80 °C at a 5 °C min^{-1} rate. The cooling rate is low from 40 °C to -40 °C to let some potential molecular species to crystallize. At the end of this process, a modulated ramp of 5 °C min^{-1} (with an oscillation period of 60 s and an amplitude of ±0.80 °C) was applied.

2.4.4. Dynamic shear rheometry (DSR).

The rheological properties of the samples were measured with a Kinexus pro+ rheometer in the shear mode, according to the EN 14770 European Standard. Each sample was loaded on a plate-plate geometry (with a diameter of 8 mm and/or 25 mm) with a 1 mm gap. The phase angle (δ) and the norm of complex modulus ($|G^*|$) were measured at high (from 20 °C to 80 °C) and low (from 20 °C down to -40 °C) temperatures, and at various frequencies (from 0.01 Hz to 10 Hz).

3. Results

3.1. Fractionation of bitumen and characterization of the resulting fractions

A 35/50 penetration grade conventional bitumen was first refluxed in *n*-pentane to separate the insoluble asphaltene fraction C_5-A. After evaporation of the solvent under reduced pressure, the *n*-pentane soluble fraction corresponding to maltenes was separated by successive chromatography (see “Bitumen fractionation procedure” in the Material and Method section) into three other fractions of increasing polarity (F_1, F_2, and F_3, respectively). Table summarizes the relative amount of these four fractions. It is noteworthy that the mass balance was not strictly equal to 100%. A mass loss of 2.1% was found after separation of C_5-A from maltenes, while

a 3.9 % loss was found after C_5-A, F1, F2 and F3 fractionation. Losses resulting from the separation process are likely due to volatile molecules lost during the evaporation of the solvents and heavy polar compounds that were not eluted during the two chromatographic steps.

Table 2. Average mass percentage (wt. %) of the four fractions resulting from the bitumen fractionation process.

C_5-A (%) (±std)	Maltenes (%) (±std)	F_1F_2 (%) (±std)	F_1 (%) (±std)	F_2 (%) (±std)	F_3 (%) (±std)
30,8 (±1.3)	67,1 (±1.6)	57 (±1)	35 (±1.2)	21,3 (±0.7)	9 (±1.4)

3.2. FT-IR characterization

The FT-IR spectra of the different fractions are presented in **Erreur ! Source du renvoi introuvable.**, showing similar features: bands at 2922 and 2850 cm^{-1} characteristic of asymmetric and symmetric stretching vibrations of C-H in $–CH_2-$ [28]; aromatic rings vibrations around 1600, 866 and 814 cm^{-1}; aliphatic vibrations of $–CH_2–$, $–CH_3$ and $–[CH_2]_n–$ at 1454, 1377 and 722 cm^{-1}, respectively [29]. In addition, F_3 presented a band at 1650 cm^{-1} probably related to stretching vibrations of C=C double bond and a stronger absorption at 1012 cm^{-1} related to sulfoxide group.

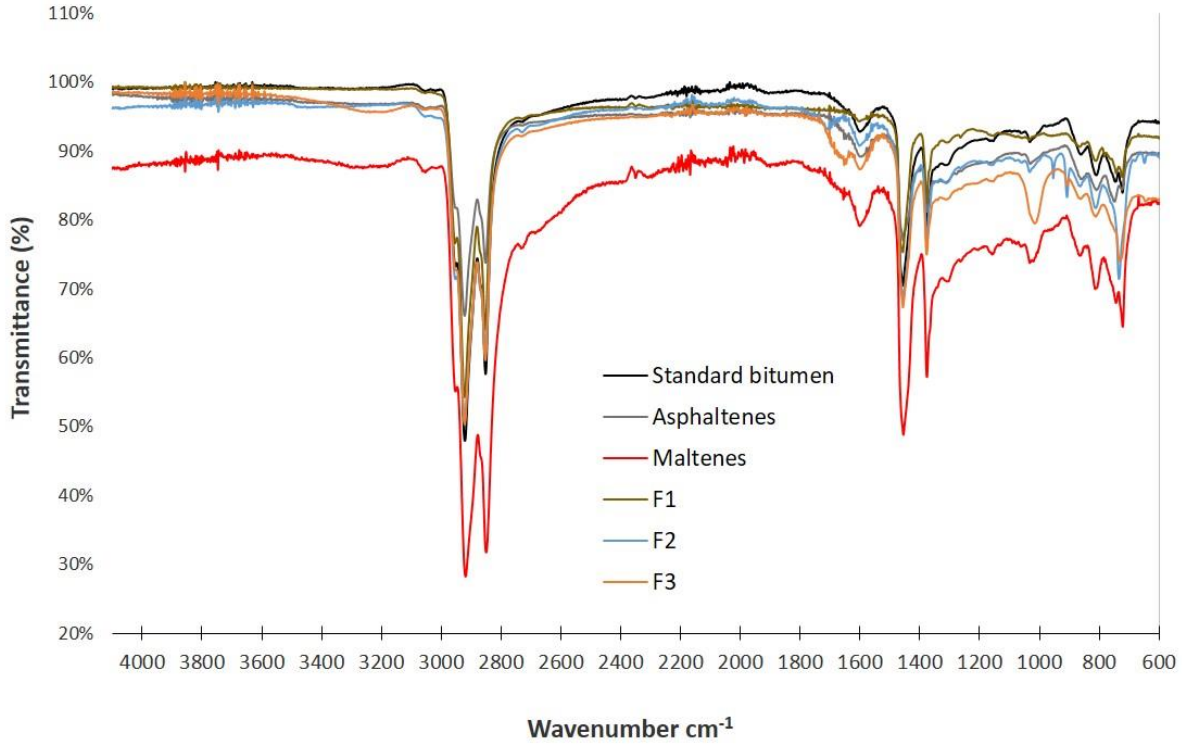

Figure 3. FT-IR spectra of the bitumen and its asphaltenes, F1, F2 and F3 fractions.

3.3. SEC characterization

Bitumen and its fractionation products were then analyzed using high-speed size exclusion chromatography (HS-SEC) to compare their molecular weight distribution. Triplicate measurements were carried out for each sample. The HS-SEC chromatograms are presented in Figure 4. Mean values of parameters describing the overall shape of the peaks are reported in Table . A very good repeatability was obtained and standard deviations showed variation coefficients around 1%. Analysis of theses parameters allowed to formulate the following assumptions:

- The UV absorbance response was strongly dependent of the tested fraction. The C_5-A fraction UV signal reached 1600 mV at the maximum while the F1 fraction reached only 313 mV. The bitumen sensitivity to UV appeared to be in-between (900mV). It has

to be noted that the F1 fraction is UV sensitive, this means that it contains some chromophore groups, maybe some unsaturated or aromatic compounds.

- The molecular weight value at the maximum of intensity allowed to rank fractions as follows (from the highest molecular weight to the lowest): C_5-A, bitumen, F3, F2, maltene, F1F2 and F1. This ranking can be explained by a simple blending mechanism. Indeed, bitumen was between C_5-A and maltenes, maltenes were between F3/F2 and F1, and F1F2 was between F2 and F1.
- As expected, a decrease of the maximum molecular weight was observed when decreasing the polarity of the maltene fractionation compounds [30]. However, distributions overlap showed that the different fractions selected by polarity did not have distinct mass distributions. The peak width at half height of the C_5-A fraction was very large (31000 g/mol) compared to others (around 5000 g/mol).
- A second molecular population was observed for both bitumen and C_5-A fractions (at 32000 and 26000 g/mol, respectively) which was not the case for the other products. As reported by Brûlé et al. [27], this peak can be assigned to asphaltene aggregates which can be observed only under the specific chromatographic conditions of HS-SEC (see Figure S2 in the SI) [27,31] whereas the weak interactions of asphaltene aggregates are broken under normal chromatography conditions. Asphaltene aggregates identified in bitumen appeared to have a highest molecular mass than asphaltene aggregates in C_5-A. The dissolution process in *n*-pentane seems to have broken some weak bonds initially present in bitumen.

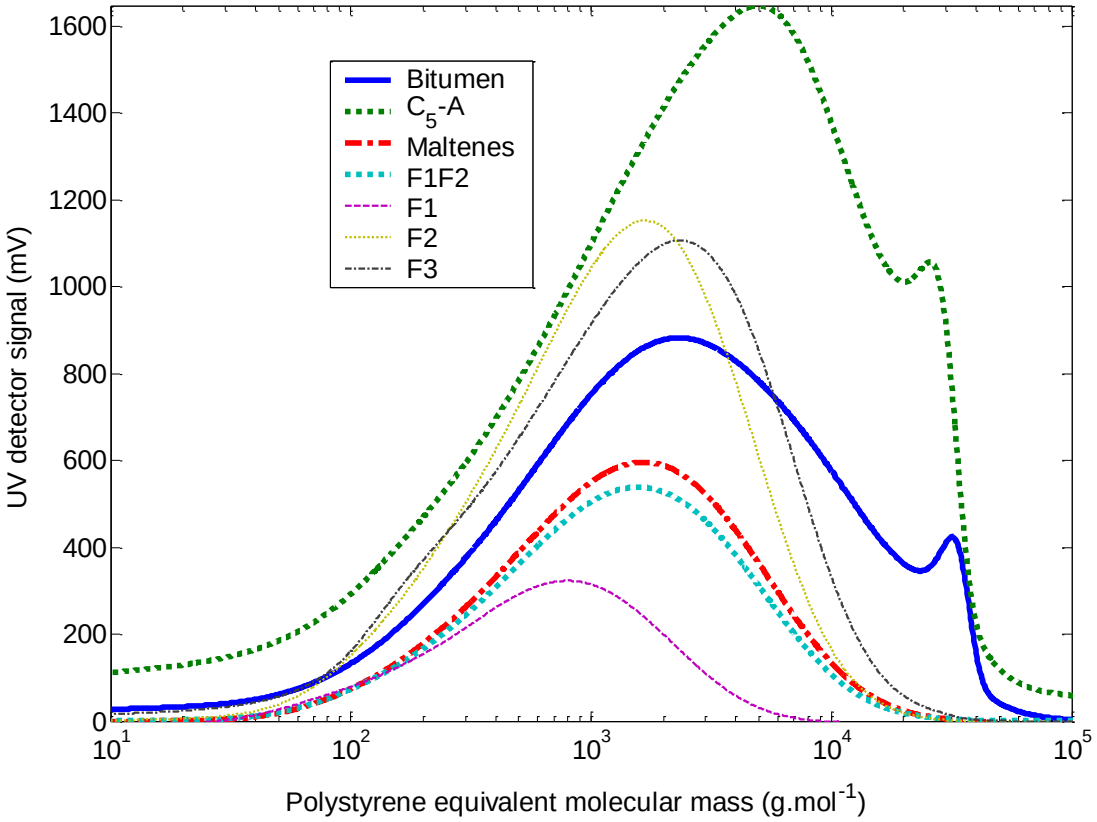

Figure 4. Molecular weight distribution measured by HS-SEC of the standard bitumen and its fractionation products (0.15 g in 10 mL of THF)

Table 3. Mean values (± standard deviation) of parameters describing the overall shape of the molecular weight distribution for the bitumen and its fractionation products

	Bitumen	**C_5-A**	**Maltenes**	**F_1F_2**	**F_1**	**F_2**	**F_3**
% (±std)	100	30.8 (±1.3)	67.1 (±1.6)	57 (±1)	35 (±1.2)	21.3 (±0.7)	9 (±1.4)
Molecular weight at the maximum of intensity (g/mol eq. PS) (±std)	2356 (±24) and 31733 (±222) [aggregates]	5042 (±81) and 25983 (±222) [aggregates]	1646 (±5)	1562 (±21)	783 (±11)	1654 (±19)	2330 (±7)

Peak width at half height (g/mol eq. PS) (±std)	14355 (±86)	30828 (±274)	5583 (±16)	5263 (±62)	2124 (±18)	4772 (±57)	7158 (±87)
UV peak (mV) (±std)	894 (±8)	1648 (±5)	594 (±1)	537 (±2)	314 (±6)	1155 (±3)	1108 (±1)

The molecular weight of the different fractions can be easily explained with polarity and blending effects (dissolution and/or thickening). However, attention must be paid concerning the fraction answer to UV at the used wavelength (340 nm being the absorption wavelength of polyaromatic compounds). It has been already reported that the UV absorption coefficient of asphaltenes is higher than the one of the whole bitumen [32]. It was assumed that the UV absorbance of the whole bitumen was a linear sum of the absorbance contribution from each fraction. In order to verify that this linear relationship could be applied on SEC chromatograms, equation 1 was applied.

$$A(MW_i) = \sum_{j=1}^{n} \alpha_j \cdot A^j(MW_i) \qquad \text{[Equation 1]}$$

Where $A^j(MW_i)$ was the UV absorbance signal of the fraction j at the molecular weight MW_i, α_j was the relative quantity of the fraction j ($with\ \sum_{j=1}^{n}(\alpha_j) = 1$) and $A(MW_i)$ was the total UV absorbance signal at the molecular weight MW_i related to the material made of the n fractions.

The verification process was as follows:

- Different fractionation cases were selected for the calculation of the theoretical chromatograms (see Table)
- α_j, α'_j α''_j , respectively fraction % related to bitumen, maltenes and F1F2, are determined by minimizing the last square error between experimental $A^{exp}(MW_i)$ and

the calculated one $A^{Cal}(MW_i)$ (by finding $min\{\sum_{i=1}^{m}(A^{exp} - A^{Cal})^2\}$). The relative mean error from the minimization procedure was given for each case in Table

- the measured and calculated α_j, α'_j α''_j coefficients were compared (Figure 5).

Figure 5 clearly shows that the calculated fractions were very close to the measured one, thus validating the assumption that the bitumen UV absorbance response was a linear sum of the absorbance contribution from each fraction.

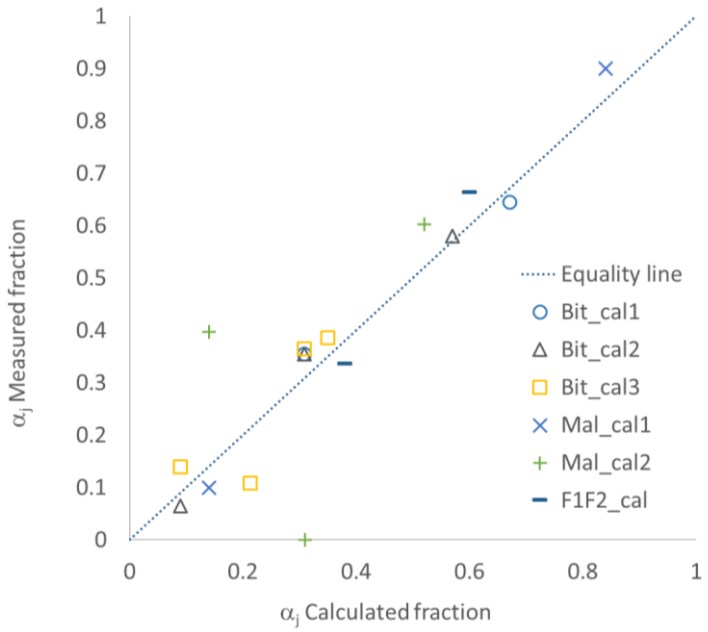

Figure 5. Comparison of measured fractions and calculated fractions α_j, α'_j, α''_j (see equation 1)

As shown in Table 5 and Figure 6, the linear combinations of the UV absorbance contribution from each fraction gave, in most cases, a good adjustment between measured and calculated chromatograms. However, this linear relationship did not work for asphaltene aggregates. In Figure , the peak attributed to asphaltene aggregates could not be reproduced by calculations,

since a difference of ca. 10000 g/mol was observed for the calculated curve compared to the measured one. Besides, when F1 was isolated, as it is the case for Bit_cal3, Mal_cal2 and F1F2_cal, the relative mean errors from the minimization procedure were higher in comparison to cases where F1 was not isolated. Moreover, this error was the highest when F1 was a large part of the material (around 50 % in maltenes and 60% in F1F2). Hence, the linear combination was strictly true for F1F2, F3 and maltenes, but not for F1 and F2, especially considering the molecular mass distribution localization. This suggested that the molecular structural arrangement in F1F2 had been destroyed after separation of F1 and F2, which leads to an underestimation of the average molecular mass when the chromatogram is calculated from the F1 and F2 molecular distribution (see Figure).

Table 4. Calculated UV absorbance cases from fractions (α, α', α'' are respectively the fraction % related to bitumen, maltenes and F1F2) and relative mean errors from the minimization procedure

		C_5-A	**Maltenes**	**F1F2**	**F1**	**F2**	**F3**	**Relative mean error (%)**
$\boldsymbol{A^{Bitumen}}$	Bit_cal1	α_{C_5-A}	$\alpha_{Maltenes}$					2.2
	Bit_cal2	α_{C_5-A}		α_{F1F2}			α_{F3}	2.3
	Bit_cal3	α_{C_5-A}			α_{F1}	α_{F2}	α_{F3}	2.8
$\boldsymbol{A^{Maltenes}}$	Mal_cal1			α'_{C_5-A}			α'_{C_5-A}	0.5
	Mal_cal2				α'_{F1}	α'_{F2}	α'_{F3}	3.3
$\boldsymbol{A^{F1F2}}$	F1F2_cal				α''_{F1}	α''_{F2}		5.4

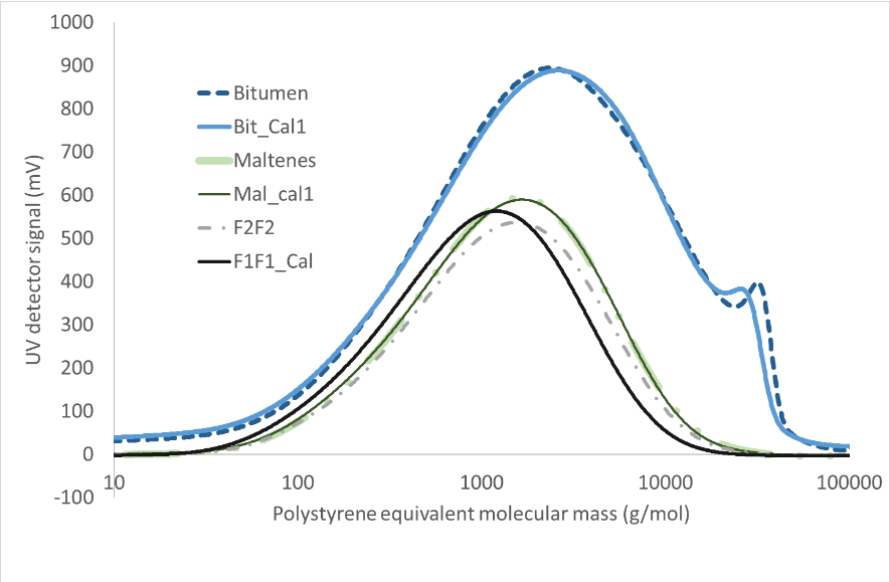

Figure 6. Measured chromatograms (dashed lines) compared to calculated one (solid lines) using equation 1 for the bitumen, maltenes and F1F2 fractions.

3.4. DSC characterization

Bitumen and its fractionation products were characterized by modulated DSC. DSC allowed to identify and quantify the material physical changes like glass transition, melting and crystallization [31-35]. Used in a modulated mode, it allowed to discriminate between both physical transitions. To achieve this, both reversible and non-reversible signals were considered. The reversible signal was attributed to the amorphous phase where the glass transition occurred, whereas the non-reversing signal showed melting/crystallization phenomena or other reordering of molecular structures [35,36].

In Figure 5, the reversible signal measured on the different fractions F1, F2, F3 and on the bitumen showed a heat flow sigmoidal decrease while temperature increased and no heat flow inflection could be observed on the signal related to asphaltenes. Hence, this confirmed that the glass transition, linked to this sigmoidal inflection, was only due to maltenes and not to asphaltenes.[37] Moreover, three distinct glass transitions were identified on signal related to F1, F2 and F3 while only one was observed for bitumen, thus meaning that the maltenic fraction,

F1, F2 and F3 were fully miscible. Tg values, calculated from the tangent methods, can be found in Table 5. The following observations can be made:

- A simple blending law was able to predict bitumen Tg from F1, F2 and F3 Tgs. 0.536*Tg midpoint (F1)+0.326*Tg midpoint (F2)+0.138*Tg midpoint (F3) = -19.0 °C which is very close to the measured value Tg midpoint (bitumen) = -19.9 °C.
- As expected, Tg values were linked to the molecular mass of the maltene fraction. As shown in **Erreur ! Source du renvoi introuvable.**, the Flory-Fox equation was validated for the F1, F2 and F3 fractions [**Erreur ! Source du renvoi introuvable.**] with a maximal asymptotic Tg value of 56 °C.
- The glass transition amplitude (Tg_{endset}-Tg_{onset}) (in °C) was highly correlated to the molecular distribution (see Figure 1).

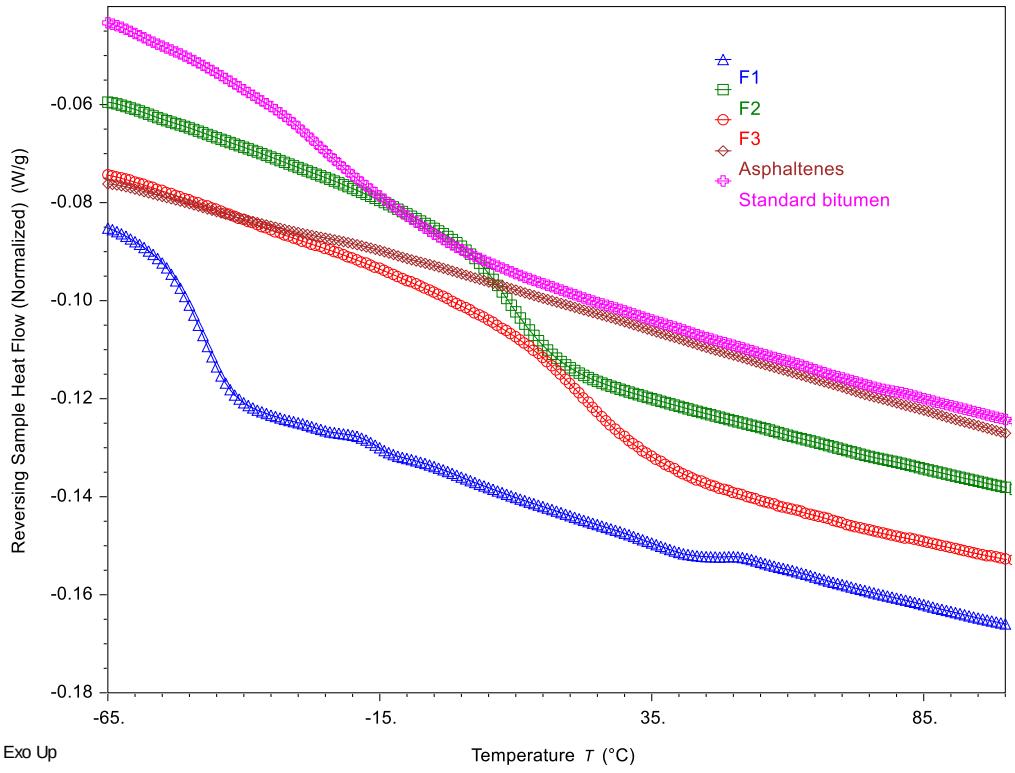

Figure 5. Reversible heat flow as a function of temperature measured in modulated differential scanning calorimetry

In Figure 6, endothermic peaks for F1, F2, F3 and also for bitumen could be observed. Once more, no physical state variations in this range of temperature were observed for asphaltenes since no endothermic peak was present. In contrast to F2 and F3, F1 showed two endothermic events. Bitumen endothermic peaks seemed to be the sum of the F1, F2 and F3 endothermic peaks.

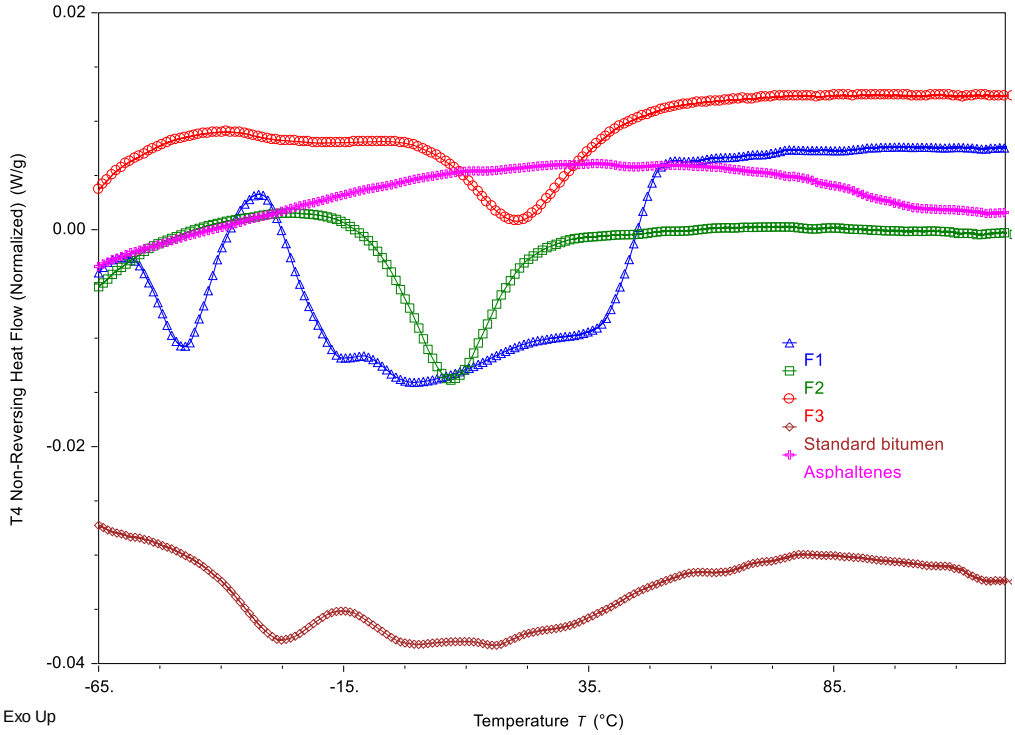

Figure 6. Non-reversible heat flow as a function of temperature measured in modulated differential scanning calorimetry

Enthalpy endotherms, attributed to crystallizable fractions, were calculated and reported in Table 5. The following observations could be made:

- Bitumen enthalpy endotherms (EE) could be calculated by a simple blending law: 0.35*EE(F1)+0.213*EE(F2)+0.09*EE(F3) = 6.3 J/g while a measured value of EE(bitumen) was equal to 6.6 J/g.

- F1 had the strongest contribution to the bitumen crystallizable fractions (around 80%).
- The F1 second endotherm was independent of the F1 glass transition ranging from -20 °C to 40 °C, and represented the major contribution to the total endotherm.

Table 5. Results from the DSC characterization of the standard bitumen and the C_5-A, F_1, F_2 and F_3 fractions.

	Tg onset (°C) (±std)	**Tg endset (°C) (±std)**	**Tg midpoint (°C) (±std)**	**ΔCp (mJ/(g.°C)) (±std)**	**Enthalpy endotherm (J/g) (±std)**
Standard bitumen	-40.66 (±1.95)	0.35 (±1.48)	-19.93 (±1.25)	474.7 (±26.9)	6.67 (±0.88)
C_5-A	\	\	\	\	\
F1	-53.26 (±0.7)	-41.85 (±0.55)	-47.56 (±0.63)	353.7 (±14.2)	15.11 (±0.31)
F2	-0.24 (±1.26)	21.12 (±0.64)	10.42 (±0.71)	395.5 (±25.5)	3.67 (±0.25)
F3	6.47 (±0.17)	39.21 (±0.88)	22.80 (±0.46)	458.3 (±5.0)	3.06 (±0.96)

3.5. Rheological characterization

The rheological properties of the standard bitumen and its fractionation products were measured in triplicate by dynamic shear rheometry (DSR). The phase angle and the norm of the complex modulus |G*| were recorded at different temperatures (from -20 to 80 °C) and at different

frequencies (from 0.01 to 10 Hz). The Black diagrams which represent the rheological signature of the samples are given in Figure 9 and consist in plotting the phase angle versus the complex modulus norm (|G*|) for an ensemble of temperature/frequency couples. Complex modulus norm isochrones (measured at 1 Hz) and phase angle are also depicted, respectively in Figure 10 and Figure 11. Standard deviations were not plotted on the figures for clarity because they were low enough.

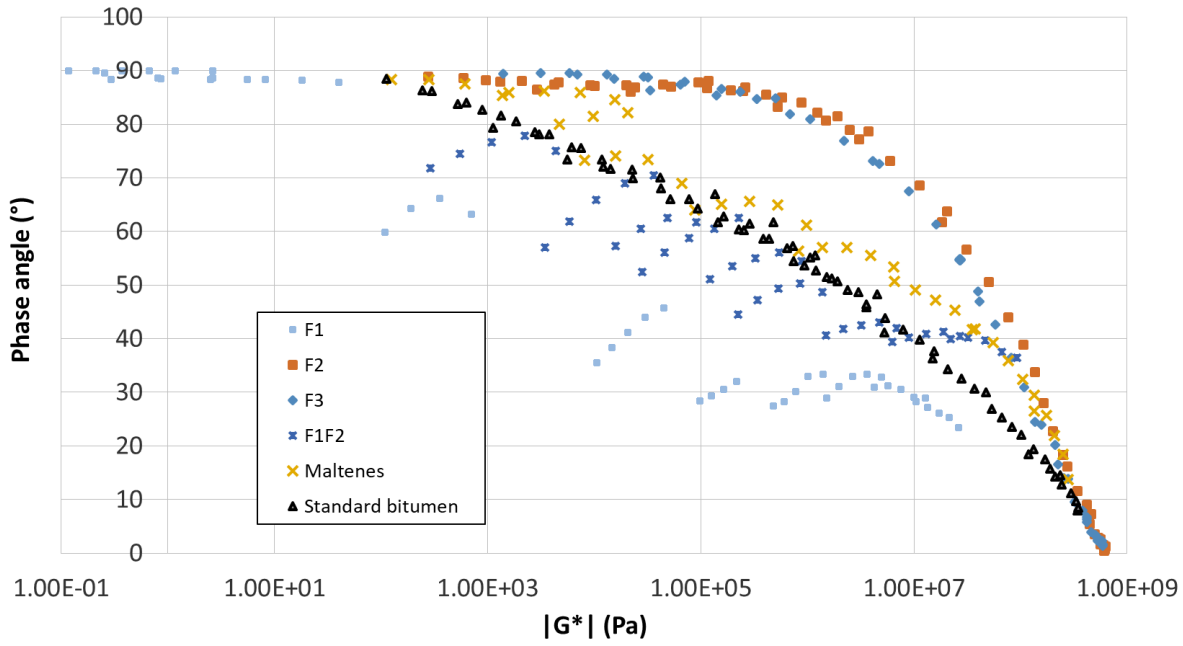

Figure 9. Complex modulus of the standard bitumen and its fractionation products, plotted in the Black space.

Figure 9 shows that the standard bitumen at low temperatures (below -20 °C) is an elastic solid characterized by a constant value of shear complex modulus (close to 1 GPa) and a low phase angle (approaching 0°) whereas at high temperatures, it is a viscous Newtonian liquid with low complex modulus values and high phase angles (nearly 90°). Between these two behaviors, the bitumen presents an intermediate viscoelastic response. Moreover, isotherms form a continuous

curve in the Black space that reflects a structural molecular organization which is thermally stable.

Figure 9 and Figure 10 clearly showed the critical role of asphaltenes in the structuration of maltenes, which contribute not only to the rigidity of the bitumen [32-34,39-40] but also to the thermal stability of the bitumen molecular structure. As an example, elimination of asphaltenes to obtain maltenes during the first fractionation step led to a decrease of the stiffness of about 2E+5 Pa at 30 °C.

A continuity of isotherms is also observed for the F_2 and F_3 Black curves (Figure 9), showing that both fractions reached a viscous liquid state at ca. 40 °C and an elastic state around -10 °C. For both fractions, endothermic peaks synchronized with the glass transition zones were observed by DSC (see Figure ***5***7 and Figure ***6*** 8). It means that the rheological thermal behavior might be driven by two simultaneous phenomena: a second order transition (glass transition) and a melting process.

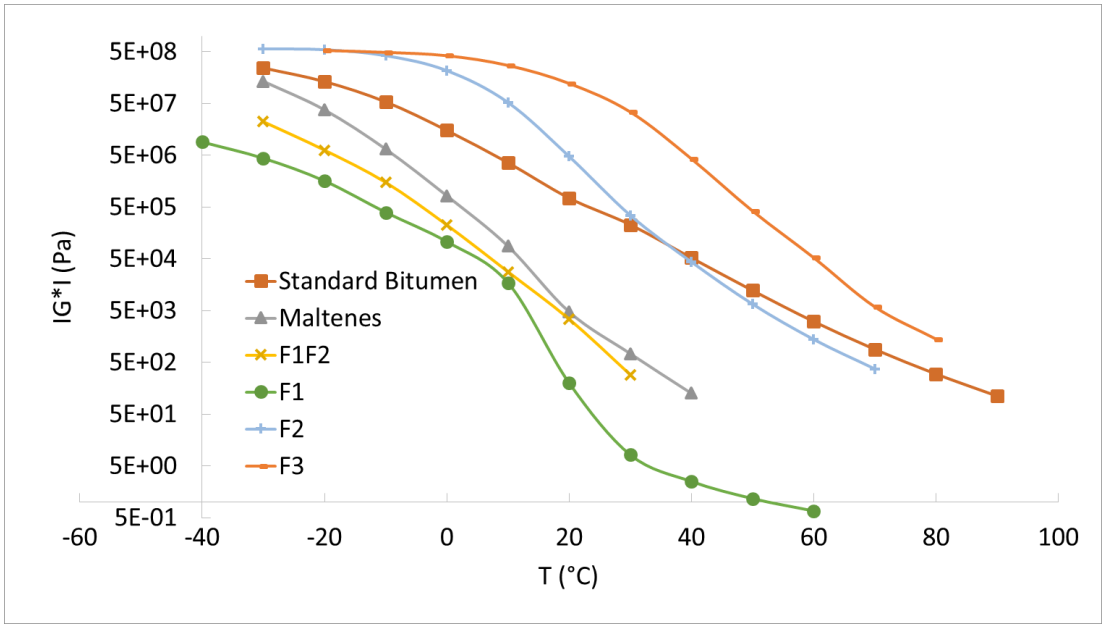

Figure 10. Norm of the complex modulus as a function of temperature (at 1 Hz) for the standard bitumen and its fractionation products.

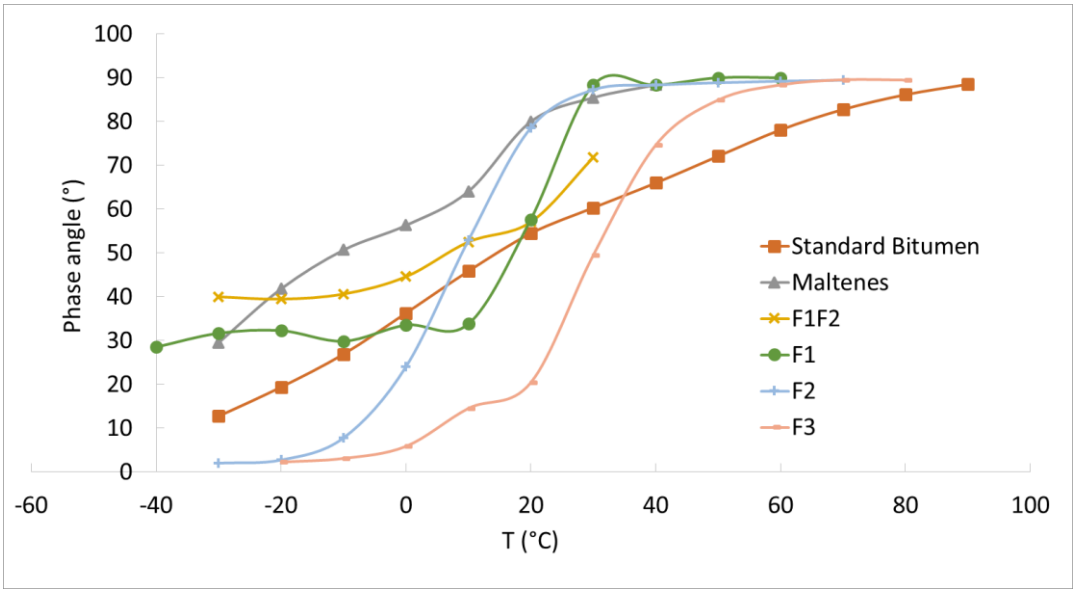

Figure 11. Phase angle as a function of temperature (at 1 Hz) for the standard bitumen and its fractionation products

Phase angle isochrones versus temperature are plotted in Figure 11, showing that the F2 and F3 rheological thermal behavior was not strictly the result of a glass transition since the phase angle exhibited a monotonic increase up to 90° instead of a well-defined peak as it is generally the case for a pure glass transition in polymers. Hence, the F2 and F3 fractions underwent a simple liquefaction process from an elastic state to a liquid viscous states upon a temperature increase, with no change in their molecular structuration.

By contrast, no continuity was observed for the maltenes, F_1F_2 and F_1 fractions. Both F1F2 and F1 fractions showed high instability toward temperature. Since F2 and F3 are thermally stable, it means that F1 was alone responsible for the maltenic fraction thermal molecular structure instability. Interestingly, although F3 fraction only accounted for 13.4 wt.% of the maltenes, it was found to structure the maltenic fraction, giving evidence of the importance of this polar fraction for the thermal stability.

The high amount of crystallizable fractions in F1 calculated from DSC (see Table 5) might be the cause of this rheological thermal instability. Indeed, a glass transition associated to an endothermic peak (see DSC measurements in Figure 7 and Figure 8) has already occurred below -40 °C. Hence, it might be assumed that above -40 °C, part of the F1 fraction has melted (as described above for F2 and F3). However, the phase angle was below 45° (Figure 11) between -40 °C and 10 °C, showing that another fraction might be responsible for this elastic response. Crystal solid particles, detected by DSC when they melt from -15 °C to 35 °C might be this fraction. Consequently it might be assumed that the binary system, composed of crystals immersed in a liquid, evolved to give less solid elastic interactions between particles when increasing the temperature. This was the reason why the rheological signature changed from a temperature to another (visible in the Black space) while in the same time the phase angle globally increased with temperature up to reach 90° due to the melting of the crystal particles (see Figure 11 and the schematic representation in Figure 12).

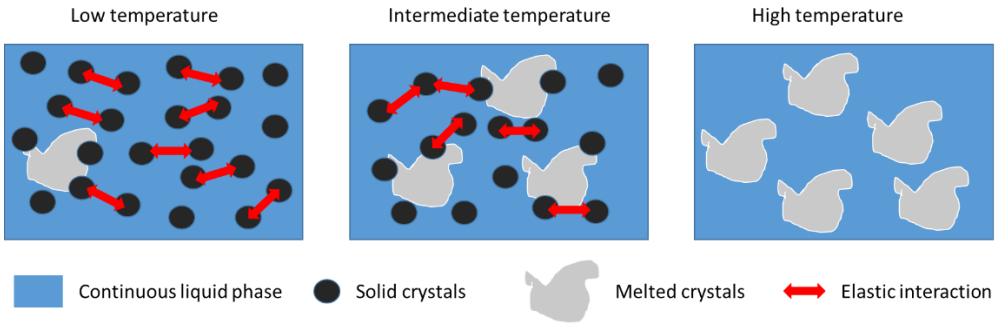

Figure 12. Schematic representation of phase structures of the F1 fraction as a function of temperature.

Finally, it is interesting to note that the complex moduli of the different fractions (Figure 10**Erreur ! Source du renvoi introuvable.**) reflected blending effects: the maltenes moduli were between those of F1, F2 and F3. The F1F2 moduli were between the F1 and F2 moduli.

Hence, these blending effects, already observed by HS-SEC and DSC, were also confirmed by modulus measurements. However, this blending principle was no more observed on the phase angle measurements (Figure 11). Indeed, maltenes phase angles were always above those of F1, F2 and F3 whereas the F1 phase angles should have been above the maltene ones if the blending principle was verified. Crystal solid particles in F1 gave less elastic contribution when there were blended with F2 and F3, in comparison to their effect when they are alone. Crystal solid particles seemed to interact with F2 and F3 molecules and let the F1 continuous liquid phase free to give the viscous behavior to the maltenic fraction.

Conclusion

A standard bitumen residue from direct crude oil distillation has been fractionated using solvents of increasing polarity using chromatographic columns. Four fractions were recovered: asphaltene, F3, F2 and F1 (from the highest to the lowest polarity). Asphaltene and F1 account for the majority of the full bitumen (31% and 35%, respectively). F3 and F2 are the intermediate fractions which account for one-third of the total, 9% and 21%, respectively. Asphaltenes were isolated as a black powder while F2 and F3 were recovered as a dark oil, and F1 as a yellow-orange light oil. In order to understand how these fractions interact together to give the final bitumen liquid viscoelastic behavior, they were characterized using infrared spectroscopy (FT-IR), size exclusion chromatography, differential scanning calorimetry (DSC) and dynamic shear rheometry (DSR). While the chemical signature given by FT-IR was similar for all fractions (even if for some peaks the intensity is different), the molecular size distribution, phase changes with temperature and rheological properties appeared to be strongly dependent of the studied fraction. From these characterizations, the following outcomes have been proposed:

- The molecular weights of the different fractions increased with the polarity of the eluting solvent. However, an overlap of the molecular weight distributions was

observed, showing that the different fractions selected by polarity have not distinct mass distributions.

- A second molecular population, assigned to asphaltene aggregates, was observed for both bitumen and asphaltene, respectively at 32000 and 26000 g/mol. The separation process of maltenes and asphaltenes in *n*-pentane seems to have altered the aggregation state initially present in bitumen, or the aggregation state is different in separated C5-asphaltenes compared to bitumen.
- The UV absorbance response in HS-SEC was strongly dependent of the fraction. Indeed, the asphaltene fraction UV absorbance response appeared to be five times more important than for F1. The UV absorbance of the whole bitumen was a linear sum of the absorbance contribution from each fraction. On a practical point of view, bitumen chromatograms obtained from SEC equipped with a UV detector have to be carefully considered, knowing that the UV coefficient absorption at a specific wavelength varies according to the polarity and the molecular weight of the sample.
- This linear relationship could be applied on SEC chromatograms and allowed calculating from a blending law the bitumen HS-SEC response. Moreover, the linear theoretical recombination applied on F1 and F2 HS-SEC chromatograms showed that a molecular structuration was destroyed when F1 and F2 were separated.
- DSC measurements confirmed that the bitumen glass transition was only due to maltenes and not to asphaltenes. Indeed, a glass transition was only observed for F1, F2 and F3 which obeyed to a simple blending law, showing that these molecules responsible for this second order phase change were fully miscible.
- Unlike F2 and F3, the F1 fraction exhibited a phase change linked to the melting of crystallizable fractions above the glass transition. A large majority of the overall bitumen crystallizable fractions were present in F1.

- Rheological characterizations showed the critical role of asphaltenes in the structuration of maltenes, which contributed not only to the rigidity of the bitumen but also to the thermal stability of the bitumen molecular structure. The F2 and F3 intermediate fractions underwent a simple liquefaction process when increasing the temperature from an elastic state to a liquid viscous state according to their molecular mass, with no changes in their molecular structuration. Crystallizable fractions, highly present in the F1 fraction, were expected to give a bitumen rheological thermal instability. However, analysis of the F1 rheological response compared to the other intermediate fractions rheological behavior, showed that crystallizable fractions interact strongly with F2 and F3 and let the F1 continuous liquid phase free to give the viscous behavior to the bitumen.

This study highlighted the importance of all bitumen phases: the less polar liquid phase driving the viscous behavior up to -50 °C, the more polar solid phase responsible of the thermal stability and the stiffness, and finally the intermediate viscous oily phases allowing the molecular weight distribution continuity and by consequence allowing to have, on a large temperature range, a viscous liquid behavior at high temperature or low frequency, and an elastic stiff behavior at low temperature. Crystallizable fractions and asphaltene aggregates seemed to act as key molecular structures in the continuous phase.

This study is limited to one type of bitumen and need to be expanded to other type of bitumen (air blown bitumen, naphtenic bitumen…).

Our future perspectives are to investigate different recombination of these fractions and study whether the rheological properties of the bitumen are preserved after a fractionation / recombination process. If such is the case, blending of phases coming from biomasses

(microalgae, vegetable oils…) of different molecular weight might be a possible option to design bitumen substitutes.

Declaration of Competing Interest

The authors declare that they have no known competing financial interests or personal relationships that could have appeared to influence the work reported in this paper.

Acknowledgement

The authors acknowledge support from IFSTTAR (doctoral grant of I. B.), and ANR (Algoroute project, grant ANR-16-CE08-0017).

References

1. Read J, Whiteoak D, Bitumen S. The Shell Bitumen Handbook. Thomas Telford; 2003.
2. Lesueur D. The colloidal structure of bitumen: Consequences on the rheology and on the mechanisms of bitumen modification. Adv Colloid Interface Sci 2009;145:42–82. https://doi.org/10.1016/j.cis.2008.08.011.
3. Saga Web n.d. https://sagaweb.afnor.org/fr-FR/sw/Consultation/Notice/1266338?directFromSearch=true (accessed October 10, 2017).
4. Goual L. Petroleum asphaltenes. Crude Oil Emuls.-Compos. Stab. Charact., InTech; 2012.
5. YEN TF, ERDMAN JG, Hanson WE. Reinvestigation of densimetric methods of ring analysis. J Chem Eng Data 1961;6:443–448.
6. Yen TF, Chilingarian GV. Asphaltenes and asphalts, 2. Elsevier; 2000.
7. Yen TF, Erdman JG, Pollack SS. Investigation of the structure of petroleum asphaltenes by X-ray diffraction. Anal Chem 1961;33:1587–1594.

8. Mullins OC. The modified Yen model. Energy Fuels 2010;24:2179–2207.
9. Spiecker PM, Gawrys KL, Kilpatrick PK. Aggregation and solubility behavior of asphaltenes and their subfractions. J Colloid Interface Sci 2003;267:178–193.
10. Groenzin H, Mullins OC. Molecular Size and Structure of Asphaltenes from Various Sources. Energy Fuels 2000;14:677–84. https://doi.org/10.1021/ef990225z.
11. Mullins OC, Sabbah H, Eyssautier J, Pomerantz AE, Barré L, Andrews AB, et al. Advances in asphaltene science and the Yen–Mullins model. Energy Fuels 2012;26:3986–4003.
12. Lesueur D. Evidence of the Colloidal Structure of Bitumen Proc. ISAP (International workshop on chemo-mechanics of bituminous materials), 2009;39-48.
13. Nellensteyn FJ. Bereiding en constitutie van asphalt. La Ruelle'sche accidenzdruckerei, Inh. Jos. Deterre & Sohn, 1923.
14. Nellensteyn FJ. The constitution of asphalt. J Inst Pet Technol 1924;10:311–323.
15. Pfeiffer JP, Saal RNJ. Asphaltic bitumen as colloid system. J Phys Chem 1940;44:139–49.
16. J.C. Petersen, R.E. Robertson, J.F. Branthaver, D.A. Anderson, D.W. Christiansen, H.U. Bahia, 1994, SHRP-A-367, Binder characterization and evaluation, Strategic Highway Research Program, National Research Council, Washington, DC.
17. Redelius PG. The structure of asphaltenes in bitumen. Road Mater Pavement Des 2006;7:143–62. https://doi.org/10.1080/14680629.2006.9690062.
18. P. Redelius, H. Soenen " Relation between bitumen chemistry and performance" Fuel 140 (2015) 34–43
19. Corbett LW. Composition of asphalt based on generic fractionation, using solvent deasphaltening, elution-adsorption chromatography, and densimetric characterization. Anal Chem 1969;41:576–579.

20. ASTM D. 4124, Standard Test Method for separation of asphalt into four fractions. Am Soc Test Mater Phila 1988.
21. Boysen RB, Schabron JF. The automated asphaltene determinator coupled with saturates, aromatics, and resins separation for heavy oil and asphalt bitumen characterization. Energy Fuels 2013; 27(8):4654–61
22. Aziz MMA, Rahman MT, Hainin MR, Abu Bakar WAW. An overview on alternative binders for flexible pavement. Constr Build Mater 2015;84:315–9. https://doi.org/10.1016/j.conbuildmat.2015.03.068.
23. Audo M, Paraschiv M, Queffelec C, Louvet I, Hemez J, Fayon F, et al. Subcritical Hydrothermal Liquefaction of Microalgae Residues as a Green Route to Alternative Road Binders. Acs Sustain Chem Eng 2015;3:583–90. https://doi.org/10.1021/acssuschemeng.5b00088.
24. Borghol I, Queffelec C, Bolle P, Descamps J, Lombard C, Lepine O, et al. Biosourced analogs of elastomer-containing bitumen through hydrothermal liquefaction of Spirulina sp microalgae residues. Green Chem 2018;20:2337–44. https://doi.org/10.1039/c8gc00094h.
25. Rosset R., Caude M., Jardy A. (1991) "Chromatographies en phases liquide et supercritique", Ed. Masson, p. 632
26. Coll H. (1971) "Behavior of micellar solutions in gel permeation chromatography. A theory based on a simple model", Gel permeation chromatography, Ed. Altgelt and Segal, Marcel publisher, 1971, pp.329-337
27. B. Brûlé, G. Ramond, C. Such (1987) Bull. Liaison Labo. P. et Ch., 148, P. 69
28. Akmaz S, Iscan O, Gurkaynak MA, Yasar M. The structural characterization of saturate, aromatic, resin, and asphaltene fractions of batiraman crude oil. Pet Sci Technol 2011;29:160–171.

29. Feng Z, Bian H, Li X, Yu J. FTIR analysis of UV aging on bitumen and its fractions. Mater Struct 2016;49:1381–9. https://doi.org/10.1617/s11527-015-0583-9.
30. Lu X, Isacsson U. Effect of ageing on bitumen chemistry and rheology. Constr Build Mater 2002;16:15–22.
31. Le Guern M, Chailleux E, Farcas F, Dreessen S, Mabille I. Physico-chemical analysis of five hard bitumens: Identification of chemical species and molecular organization before and after artificial aging. Fuel 2010;89:3330–9. https://doi.org/10.1016/j.fuel.2010.04.035.
32. Albert M. Hung, Ellie H. Fini, Absorption spectroscopy to determine the extent and mechanisms of aging in bitumen and asphaltenes. Fuel 241 (2019) 408-415
33. Xiaokong Yu, Nancy A. Burnham, Sergio Granados-Focil, Mingjiang Tao, Bitumen's microstructures are correlated with its bulk thermal and rheological properties, Fuel 254 (2019)
34. Planche JP, Claudy PM, Létoffé JM, Martin D. Using thermal analysis methods to better understand asphalt rheology. Thermochim Acta 1998;324:223–227.
35. Masson J.F., Polomark G.M., "Bitumen Microstructure by Modulated Differential Scanning Calorimetry", Thermochim Acta, Vol. 374, No. 2, 2001, p. 105-114.
36. Pavel Kriz , Jiri Stastna & Ludo Zanzotto, Glass Transition and Phase Stability in Asphalt Binders, Road Materials and Pavement Design. EATA 2008, pages 37 to 65
37. P. Claudy , J.M. Letoffe , G.N. King , J.P. Planch, B. Brule "Characterization of paving asphalts by differential scanning calorimetry" Fuel Sci. Technol. Intern. 1991, 9:1, 71-92.
38. T.G. Fox et P.J. Flory, Second-order transition temperatures and related properties of polystyrene, Journal of Applied Physics, volume 21, pages 581–591, 1950

39. Hofko B, Eberhardsteiner L, Fuessl J, Grothe H, Handle F, Hospodka M, et al. Impact of maltene and asphaltene fraction on mechanical behavior and microstructure of bitumen. Mater Struct 2016;49:829–41. https://doi.org/10.1617/s11527-015-0541-6.

40. Eberhardsteiner L, Fuessl J, Hofko B, Handle F, Hospodka M, Blab R, et al. Influence of asphaltene content on mechanical bitumen behavior: experimental investigation and micromechanical modeling. Mater Struct 2015;48:3099–112. https://doi.org/10.1617/s11527-014-0383-7.